



# Syntheses, crystal structure, photophysical property and theoretical study of a new series of iridium complexes with *N*-(diphenylphosphoryl)benzamide derivatives as the ancillary ligands

Tian-Yi Li<sup>a</sup>, Xiao Liang<sup>a</sup>, Chen Wu<sup>a</sup>, Li-Sha Xue<sup>a</sup>, Qiu-Lei Xu<sup>a</sup>, Song Zhang<sup>a</sup>, Xuan Liu<sup>a</sup>, You-Xuan Zheng<sup>a,\*</sup>, Xiu-Qiang Wang<sup>b,\*\*</sup>

<sup>a</sup>State Key Laboratory of Coordination Chemistry, Nanjing National Laboratory of Microstructures, School of Chemistry and Chemical Engineering, Center for Molecular Organic Chemistry, Nanjing University, Nanjing 210093, PR China

<sup>b</sup>School of Life Science, Nanjing University, Nanjing 210093, PR China

## ARTICLE INFO

### Article history:

Received 29 October 2013

Received in revised form

3 January 2014

Accepted 14 January 2014

### Keywords:

Iridium(III) complex

*N*-(Diphenylphosphoryl)benzamide

Ancillary ligand

Photoluminescence

Computational calculation

## ABSTRACT

Seven iridium complexes with the general structure of **(tfmpppy)<sub>2</sub>Ir(L1–L7)** (tfmpppy = 4-trifluoromethyl phenylpyridine) were synthesized, where ancillary ligands **L1–L7** are fluorine- or trifluoromethyl-substituted (–F or –CF<sub>3</sub>) *N*-(diphenylphosphoryl)benzamide derivatives. Single crystal X-ray diffraction study was undertaken on all complexes, which showed that each adopted the distorted octahedral coordination geometry with the conventional *trans*-N, *cis*-C arrangement in the coordination sphere. Electrochemical study confirmed the electron-withdrawing –F and –CF<sub>3</sub> substituents on the ancillary ligands have effects on the Ir<sup>III/IV</sup> redox couples and HOMO/LUMO energy levels. Density functional theory (DFT) calculation results showed that the HOMOs are composed of Ir 5*d* orbital (about 55%) and  $\pi$  orbitals of the phenyl rings (about 38%) in tfmpppy ligands, whilst the LUMOs are mostly localized on both the phenyl and pyridine rings of tfmpppy (about 90%). All the complexes own the similar emission peaks around 520 nm with short phosphorescent decay time about 2  $\mu$ s at ambient temperature and relatively high internal quantum efficiencies from 37.5 to 61.2%. This work showed that the iridium complexes with *N*-(diphenylphosphoryl)benzamide derivatives as the ancillary ligands possess the potential as phosphorence dopants in the organic light-emitting diodes (OLEDs).

© 2014 Elsevier B.V. All rights reserved.

## 1. Introduction

The iridium complexes with heterocyclic ligands have found a wide range of applications in the context of photoactive molecular materials. The strong spin-orbit coupling (SOC) introduced by the central heavy atom can promote the triplet to singlet radiative transition, so that such complexes may exhibit unusually high phosphorescence quantum yields at ambient temperature, as well as relatively short triplet lifetimes. In addition, inter-system crossing (ISC) from the first singlet excited state (*S*<sub>1</sub>) to the triplet state (typically *T*<sub>1</sub>) also can be accelerated. Since *S*<sub>1</sub> is depopulated at a rate ( $10^{12} \text{ s}^{-1}$ ) much faster than that of phosphorescent radiative emission rate ( $10^8\text{--}10^9 \text{ s}^{-1}$ ) [1], fluorescence is depressed in

these iridium complexes and triplet harvest can be expected, which is advantageous to the emission from the triplet excited states, and to obtain a relatively high quantum yield (100% theoretically). On the other hand, since the phosphorescence of iridium complexes primarily originates from the triplet metal-to-ligand charge-transfers (<sup>3</sup>MLCT) and the ligand-centered (<sup>3</sup>LC) transitions states [2], the energy level of the excited state can be controlled by tuning the energy levels of the ligands through substituent effects, which leads to a wide flexible emission color range. Thus, such iridium complexes have been widely studied for photocatalysts [3], photochemical solar energy conversion [4], biological labels [5] and, in particular, phosphorescent dopants in the organic light-emitting diodes (OLEDs) [6–9].

In pursuit of highly emissive iridium complexes, many heteroleptic complexes with the structure of Ir(CN)<sub>2</sub>(LX) have been developed, where CN is a monoanionic cyclometallated ligand (e.g., phenylpyridine (ppy), 4-trifluoromethylphenylpyridine (tfmpppy)) and LX stands for an ancillary ligand (e.g., acetylacetonate (acac), picolinate (pic)). With the help of the density functional theory

\* Corresponding author. Tel.: +86 25 83596775; fax: +86 25 83314502.

\*\* Corresponding author.

E-mail addresses: [yxzheng@nju.edu.cn](mailto:yxzheng@nju.edu.cn) (Y.-X. Zheng), [xqwang@nju.edu.cn](mailto:xqwang@nju.edu.cn) (X.-Q. Wang).

(DFT) and the time-dependent DFT (TD-DFT) calculations, an insight of the photophysical property in such complexes reveals that the highest occupied molecular orbital (HOMO) is usually dominated by the central iridium atom, whereas the lowest unoccupied molecular orbital (LUMO) is primarily localized on the cyclometallated ligands. As a result, heteroleptic complexes own the similar phosphorescence profile as that of the previously popular *fac*-tris(cyclometallated (*fac* = facial) iridium complexes [2,10]. Although ancillary ligand does not make contribution to the lowest excited state directly, it indeed alters the energy levels of the excited states by modifying the electron density at the metal center. Thus, the photophysical property and carrier mobility of iridium complexes can be tuned through functional substitutes on both cyclometallated and ancillary ligands.

According to this guideline, our group have proved that the heteroleptic complex (tfmppy)<sub>2</sub>Ir(tpip) (tpip = tetraphenylimido diphosphinate) possesses valuable properties for electroluminescent devices, such as high quantum yield, short lifetime and high electron transition mobility, due to the newly developed ancillary ligand tpip with greater polar P=O moieties [11–13]. In this paper, on the basis of tetraphenylimidodiphosphinate, we altered one of the P=O moiety to C=O moiety and synthesized a new series of *N*-(diphenylphosphoryl)benzamide derivatives, **L1–L7**, as the ancillary ligands and their corresponding iridium complexes, **Ir1–Ir7**, with 4-trifluoromethylphenylpyridine as the cyclometallated ligands. This paper presents the syntheses, crystal structures and spectroscopic property of these iridium complexes, together with detailed theoretical study.

## 2. Experimental section

### 2.1. General information

All reactions were performed under nitrogen atmosphere. Reactants were used without further purification as commercial grade. Organic solvents for synthetic reactions were carefully dried and distilled prior to use. <sup>1</sup>H NMR (DMSO-*d*<sub>6</sub>) and <sup>13</sup>C NMR (CDCl<sub>3</sub>) spectra were run on a Bruker AM 500 and a Bruker AM 300 spectrometer, respectively. The chemical shifts ( $\delta$ ) were given in ppm based on internal TMS. The mass spectrometry (MS) spectra were obtained on an electrospray ionization (ESI) mass spectrometer (LCQ fleet, Thermo Fisher Scientific) for ligands. The high resolution mass spectra measurements (HR EI-MS) were recorded on an Agilent 6540 UHD Accurate-Mass Q-TOF LC/MS for all materials. Melting points (M.p.) were determined on a Focus X-4 micro melting point apparatus. Elemental analyses for C, H, and N were performed on an Elementar Vario MICRO analyzer. Cyclic voltammogram (CV) curves were recorded at room temperature under nitrogen protection in deaerated acetonitrile, using a three-electrode cell equipped with a Pt disk working electrode, a Pt wire counter electrode, and a Ag<sup>+</sup>/Ag reference electrode on a computer-controlled IM6ex electrochemical and chemiluminescent system (Zahner) using *tetra*-*n*-butylammoniumperchlorate (0.1 M) as the supporting electrolyte with a potential scan rate of 50 mV s<sup>-1</sup> during the measurements. All potentials are calibrated with Fc<sup>+</sup>/Fc in acetonitrile as a reference. UV–vis absorption spectra were measured on a Shimadzu UV-3100 spectrophotometer as CH<sub>2</sub>Cl<sub>2</sub> solutions (5.0 × 10<sup>-6</sup> M). Photoluminescence (PL) spectra were obtained on a Hitachi F-4600 PL spectrometer as deaerated CH<sub>2</sub>Cl<sub>2</sub> solutions (5.0 × 10<sup>-5</sup> M) at room temperature and 77 K, as well as for the neat solid powders. Neither emission nor excitation spectra were corrected. Luminescence lifetime curves were measured on an Edinburgh Instruments FLS920P fluorescence spectrometer and the data were treated as one-order exponential fitting using OriginPro 8 software.

The luminescence quantum efficiencies were calculated by a comparison of the emission intensities (integrated areas) of a standard sample *fac*-Ir(ppy)<sub>3</sub> and the unknown samples in deaerated acetonitrile solutions of 5 × 10<sup>-5</sup> mol L<sup>-1</sup> according to the Eq. [14–16]

$$\Phi_{\text{unk}} = \Phi_{\text{std}} \left( \frac{I_{\text{unk}}}{I_{\text{std}}} \right) \left( \frac{A_{\text{std}}}{A_{\text{unk}}} \right) \left( \frac{\eta_{\text{unk}}}{\eta_{\text{std}}} \right)^2$$

where  $\Phi_{\text{unk}}$  and  $\Phi_{\text{std}}$  are the luminescence quantum yield values of the unknown samples and *fac*-Ir(ppy)<sub>3</sub> solutions ( $\Phi_{\text{std}} = 40\%$  [16]), respectively.  $I_{\text{unk}}$  and  $I_{\text{std}}$  are the integrated emission intensities of the unknown samples and *fac*-Ir(ppy)<sub>3</sub> solutions, respectively.  $A_{\text{unk}}$  and  $A_{\text{std}}$  are the absorbance values of the unknown samples and *fac*-Ir(ppy)<sub>3</sub> solutions at their excitation wavelengths, respectively.  $\eta_{\text{unk}}$  and  $\eta_{\text{std}}$  terms represent the refractive indices of the corresponding acetonitrile (1.345, pure solvent was assumed).

### 2.2. Crystallography

Diffraction data for **Ir1**, **Ir2**, **Ir3**, **Ir4**, **Ir5**, **Ir6** and **Ir7** were collected on a Siemens (Bruker) SMART CCD diffractometer using monochromated Mo-K $\alpha$  radiation ( $\lambda = 0.71073$  Å) at room temperature. Cell parameters were retrieved using SMART software, and SAINT [17] program was used to reduce the highly redundant data sets. Lorentz and polarization effects were corrected. Absorption corrections were performed with SADABS [18] supplied by Bruker. Data were collected using a narrow-frame method with scan widths of 0.30 ° in  $\omega$  and an exposure time of 4 s frame<sup>-1</sup>.

The molecular structures were solved by direct methods and refined by full-matrix least squares on  $F^2$  using the program SHELXL-97 [19]. The positions of the metal atoms and their conjoint coordination atoms were located by the Patterson method directly on E-maps; other non-H atoms were found in alternating difference Fourier syntheses and least-squares refinement cycles. All non-H atoms were treated anisotropically. H atoms were fixed in calculated positions and they were allowed to ride on their parent C atoms and refined with a uniform value of  $U_{\text{iso}}$ . Where the structures are disordered, various geometrical (SADI) and displacement (SIMU) restrictive parameters were employed to obtain more reasonable structures.

### 2.3. Computational details

Full geometry optimizations of the complexes in the singlet ground-state were carried out using density functional theory (DFT) method [20]. The Beche's LYP (B3LYP) [21–23] exchange-correlation functional was employed, which had been proven to be efficient for the geometry optimization of complexes with heavy metals [24,25]. No symmetry constraint was applied during the geometry optimizations. On the basis of the optimized molecular structures, the absorption properties in CH<sub>2</sub>Cl<sub>2</sub> were studied by time-dependent DFT (TD-DFT) [26,27] method using both B3LYP and M06-2x [28] exchange-correlation functional, and the solvent effect of CH<sub>2</sub>Cl<sub>2</sub> was taken into consideration with the appliance of the conductor-like polarizable continuum model (C-PCM) [29]. To cover the experimental range, the first 60 vertical excitations were taken into consideration and only the spin-allowed singlet–singlet transitions were calculated. Concerning the basis sets, a “double- $\xi$ ” quality basis set LANL2DZ [30] was used for iridium atom and the 6-31G(d,p) [31] basis set was employed for other non-metal atoms through the process of all the calculations.

All the calculations were carried out with Gaussian 09 software package [32]. GaussSum 2.2 program [33] was used for the stimulations (simulated with Gaussian distribution with a Full Width at

Half-Maximum set FWHM = 5000 cm<sup>-1</sup>) and analyses of electronic absorption spectra. QMForge program was used to give accurate percentage data of frontier molecular orbitals.

## 2.4. Syntheses

The syntheses routes of the tfmpppy main ligand [11], seven ancillary ligands of N-(diphenylphosphoryl)benzamide derivatives **L1–L7** [34], and the corresponding iridium complexes **Ir1–Ir7** are shown in Scheme 1.

### 2.4.1. General syntheses of **L1–L7** ligands

Benzamide derivatives (5.00 mmol), DMAP (*N,N*-dimethylpyridin-4-amine, 8.00 mmol) and chlorodiphenylphosphine derivatives (5.00 mmol) were dissolved in anhydrous THF (20 mL) and refluxed for 10 h. The mixtures were filtered to remove the white byproducts and the rapid column chromatography (silica, petroleum ether:EtOAc = 3:1) of the solutions gave the white intermediate products. Then, 0.5 mL 30% H<sub>2</sub>O<sub>2</sub> was added into the intermediate products THF solutions to give the target products as white powders after stirring for 2 h at room temperature.

**L1** [34]. 0.60 g Benzamide and 1.10 g chlorodiphenylphosphine gave 0.75 g **L1** (2.34 mmol, 46.8%). M.p.: 167–169 °C. <sup>1</sup>H NMR (500 MHz, DMSO-*d*<sub>6</sub>) δ 10.30 (d, *J* = 8.9 Hz, 1H), 7.98 (d, *J* = 7.7 Hz, 2H), 7.86 (dd, *J* = 12.4, 7.8 Hz, 4H), 7.63 (d, *J* = 7.5 Hz, 1H), 7.58 (d, *J* = 7.2 Hz, 2H), 7.54 (d, *J* = 3.0 Hz, 2H), 7.53–7.50 (m, 4H). MS (ESI) Calcd for [M – H]<sup>-</sup>: *m/z* 320.3, found: *m/z* 320.2. HR EI-MS Calcd for [M + H]<sup>+</sup>: *m/z* 322.0991, found: *m/z* 322.0994.

**L2**. 0.60 g Benzamide and 1.28 g chlorobis(4-fluorophenyl)phosphine gave 0.77 g **L2** (2.17 mmol, 43.3%). M.p.: 182–184 °C. <sup>1</sup>H NMR (500 MHz, DMSO-*d*<sub>6</sub>) δ 10.33 (d, *J* = 8.9 Hz, 1H), 7.97 (d, *J* = 7.7 Hz, 2H), 7.96–7.87 (m, 4H), 7.63 (t, *J* = 7.3 Hz, 1H), 7.51 (t,

*J* = 7.6 Hz, 2H), 7.38 (t, *J* = 8.0 Hz, 4H). MS (ESI) Calcd for [M – H]<sup>-</sup>: *m/z* 356.3, found: *m/z* 356.2. HR EI-MS Calcd for [M + Na]<sup>+</sup>: *m/z* 380.0622, found: *m/z* 380.0622.

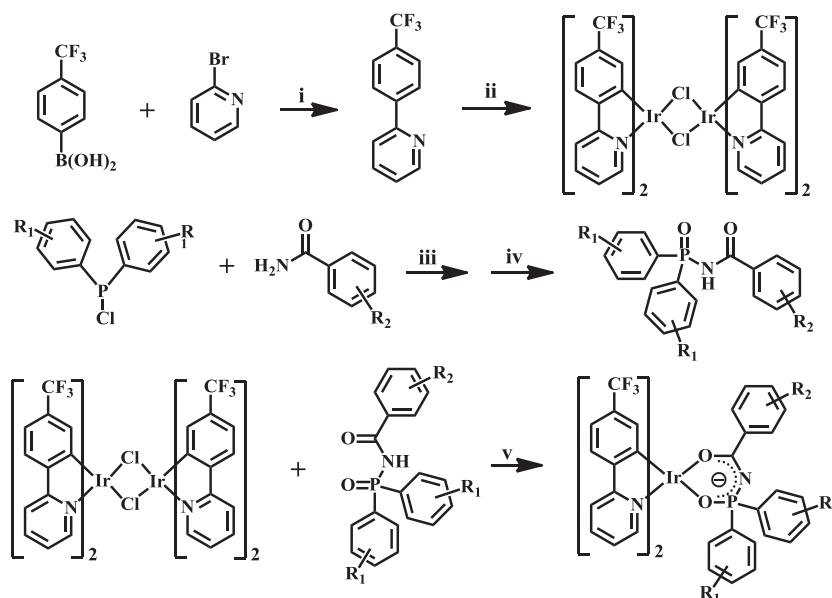
**L3**. 0.60 g Benzamide and 1.78 g chlorobis(4-(trifluoromethyl)phenyl)phosphine gave 0.76 g **L3** (1.66 mmol, 33.1%). M.p.: 159–161 °C. <sup>1</sup>H NMR (500 MHz, DMSO-*d*<sub>6</sub>) δ 10.61 (d, *J* = 9.4 Hz, 1H), 8.14 (dd, *J* = 11.8, 8.3 Hz, 4H), 8.00 (d, *J* = 7.7 Hz, 2H), 7.93 (d, *J* = 7.1 Hz, 4H), 7.66 (t, *J* = 7.3 Hz, 1H), 7.54 (t, *J* = 7.6 Hz, 2H). MS (ESI) Calcd for [M – H]<sup>-</sup>: *m/z* 456.3, found: *m/z* 456.3. HR EI-MS Calcd for [M + Na]<sup>+</sup>: *m/z* 480.0559, found: *m/z* 480.0559.

**L4**. 0.88 g 3,4,5-Trifluorobenzamide and 1.10 g chlorodiphenylphosphine gave 0.89 g **L4** (2.36 mmol, 47.3%) as white powder. M.p.: 182–184 °C. <sup>1</sup>H NMR (500 MHz, DMSO-*d*<sub>6</sub>) δ 10.45 (s, 1H), 8.03–7.93 (m, 2H), 7.89 (dd, *J* = 12.4, 7.6 Hz, 4H), 7.60 (t, *J* = 7.0 Hz, 2H), 7.58–7.50 (m, 4H). MS (ESI) Calcd for [M – H]<sup>-</sup>: *m/z* 374.3, found: *m/z* 374.2. HR EI-MS Calcd for [M + Na]<sup>+</sup>: *m/z* 398.0528, found: *m/z* 398.0528.

**L5**. 0.70 g 4-Fluorobenzamide and 1.10 g chlorodiphenylphosphine gave 0.63 g **L5** (1.85 mmol, 37.0%). M.p.: 189–191 °C. <sup>1</sup>H NMR (500 MHz, DMSO-*d*<sub>6</sub>) δ 10.34 (s, 1H), 8.06 (s, 2H), 7.87 (s, 4H), 7.58 (d, *J* = 4.7 Hz, 2H), 7.53 (s, 4H), 7.35 (s, 2H). MS (ESI) Calcd for [M – H]<sup>-</sup>: *m/z* 338.3, found: *m/z* 338.2. HR EI-MS Calcd for [M + H]<sup>+</sup>: *m/z* 340.0897, found: *m/z* 340.0898.

**L6**. 0.88 g 3,4,5-Trifluorobenzamide and 1.28 g chlorobis(4-fluorophenyl)phosphine gave 0.44 g **L6** (1.08 mmol, 21.5%). M.p.: 176–179 °C. <sup>1</sup>H NMR (500 MHz, DMSO-*d*<sub>6</sub>) δ 10.49 (s, 1H), 8.02–7.96 (m, 4H), 7.94 (s, 2H), 7.39 (t, *J* = 8.1 Hz, 4H). MS (ESI) Calcd for [M – H]<sup>-</sup>: *m/z* 410.3, found: *m/z* 410.2. HR EI-MS Calcd for [M + Na]<sup>+</sup>: *m/z* 434.0340, found: *m/z* 434.0340.

**L7**. 0.70 g 4-Fluorobenzamide and 1.28 g chlorobis(4-fluorophenyl)phosphine gave 0.36 g **L7** (0.971 mmol, 19.4%). M.p.: 112–115 °C. <sup>1</sup>H NMR (500 MHz, DMSO-*d*<sub>6</sub>) δ 10.36 (d, *J* = 8.7 Hz, 1H),



**L1, Ir1:** R<sub>1</sub>=H, R<sub>2</sub>=H; **L2, Ir2:** R<sub>1</sub>=4-F, R<sub>2</sub>=H; **L3, Ir3:** R<sub>1</sub>=4-CF<sub>3</sub>, R<sub>2</sub>=H;  
**L4, Ir4:** R<sub>1</sub>=H, R<sub>2</sub>=3,4,5-F; **L5, Ir5:** R<sub>1</sub>=H, R<sub>2</sub>=4-F;  
**L6, Ir6:** R<sub>1</sub>=4-F, R<sub>2</sub>=3,4,5-F; **L7, Ir7:** R<sub>1</sub>=4-F, R<sub>2</sub>=4-F.

(i) Pt(PPh<sub>3</sub>)<sub>4</sub>, K<sub>2</sub>CO<sub>3</sub>, THF, H<sub>2</sub>O, reflux, 12 h; (ii) IrCl<sub>3</sub>·H<sub>2</sub>O, EtOEtOH, H<sub>2</sub>O, 110 °C, 12 h;  
 (iii) THF, DMAP, reflux, 10 h; (iv) H<sub>2</sub>O<sub>2</sub>, THF, room temperature; (v) Potassium *t*-butoxide, EtOEtOH, 120 °C, 12 h.

Scheme 1. Synthetic routes of the ligands and complexes.

8.06 (dd,  $J = 8.4, 5.6$  Hz, 2H), 7.94 (dt,  $J = 13.7, 7.2$  Hz, 4H), 7.41 (d,  $J = 12.5$  Hz, 2H), 7.39–7.34 (m, 4H). MS (ESI) Calcd for  $[M - H]^-$ :  $m/z$  374.3, found:  $m/z$  374.2. HR EI-MS Calcd for  $[M + Na]^+$ :  $m/z$  398.0528, found:  $m/z$  398.0528.

#### 2.4.2. General syntheses of iridium complexes **Ir1**–**Ir7**

$\text{IrCl}_3 \cdot 3\text{H}_2\text{O}$  (1.76 g, 5.0 mmol) and **tfmppy** (2.45 g, 11.0 mmol) in 6.0 mL 2-ethoxyethanol and 3.0 mL distilled water were heated at 120 °C for 12 h. After the solution was cooled, the addition of 30 mL water gave a bright yellow precipitate which was filtered and washed with distilled water and ethanol, yielding 3.09 g  $[(\text{tfmppy})_2\text{Ir}(\mu\text{-Cl})_2]$  (2.30 mmol, 92.0%). The  $\mu$ -chloro-bridged dimer complex was used for the subsequent reaction without characterization and further purification.  $[(\text{tfmppy})_2\text{Ir}(\mu\text{-Cl})_2]$  (0.40 g, 0.30 mmol) and **L1**–**L7** (0.65 mmol) in 5 mL 2-ethoxyethanol were heated at 120 °C. Potassium *tert*-butoxide (0.07 g, 0.65 mmol) in 5.0 mL MeOH was injected into the mixtures dropwise. After 12 h, the precipitates were filtered, washed with ethanol and gave the products as bright yellow powders. The pure complexes were obtained from recrystallization by using solvent diffusion of MeOH into  $\text{CH}_2\text{Cl}_2$  solutions.

**(tfmppy)<sub>2</sub>Ir(L1) (Ir1)**. 0.40 g  $[(\text{tfmppy})_2\text{Ir}(\mu\text{-Cl})_2]$  and 0.21 g **L1** (0.65 mmol) gave 0.37 g **Ir1** (0.38 mmol, 63.8%).  $^1\text{H}$  NMR (500 MHz,  $\text{CDCl}_3$ )  $\delta$  8.37 (d,  $J = 5.6$  Hz, 1H), 8.00 (d,  $J = 7.5$  Hz, 2H), 7.93 (d,  $J = 7.7$  Hz, 1H), 7.90 (d,  $J = 8.1$  Hz, 2H), 7.85 (d,  $J = 8.1$  Hz, 1H), 7.75 (t,  $J = 7.4$  Hz, 1H), 7.69 (d,  $J = 8.1$  Hz, 1H), 7.65 (d,  $J = 8.1$  Hz, 1H), 7.54 (t,  $J = 7.4$  Hz, 1H), 7.42 (dt,  $J = 13.1, 7.5$  Hz, 6H), 7.31 (d,  $J = 7.6$  Hz, 2H), 7.28–7.23 (m, 2H), 7.16 (t,  $J = 6.7$  Hz, 2H), 7.12 (d,  $J = 8.1$  Hz, 1H), 7.08 (td,  $J = 7.6, 3.0$  Hz, 2H), 6.57 (t,  $J = 6.5$  Hz, 1H), 6.52 (s, 1H), 6.29 (s, 1H).  $^{13}\text{C}$  NMR (75 MHz,  $\text{CDCl}_3$ )  $\delta$  206.90, 174.53, 166.77, 149.72, 149.31, 145.33, 143.80, 137.48, 137.05, 131.04, 130.92, 130.85, 130.76, 130.64, 129.16, 128.36, 128.11, 127.95, 127.64, 123.34, 123.24, 122.74, 122.32, 119.03, 118.68, 118.11. HR EI-MS Calcd for  $[M + H]^+$ :  $m/z$  958.1604, found:  $m/z$  958.1604. Anal. calcd for  $\text{C}_{43}\text{H}_{29}\text{O}_2\text{N}_3\text{PF}_6\text{Ir}$ : C 53.97, N 4.39, H 3.05. Found: C 53.68, N 4.24, H 3.35.

**(tfmppy)<sub>2</sub>Ir(L2) (Ir2)**. 0.40 g  $[(\text{tfmppy})_2\text{Ir}(\mu\text{-Cl})_2]$  and 0.23 g **L2** gave 0.48 g **Ir2** (0.48 mmol, 80.3%).  $^1\text{H}$  NMR (500 MHz,  $\text{CDCl}_3$ )  $\delta$  9.17 (d,  $J = 5.6$  Hz, 1H), 8.36 (d,  $J = 5.5$  Hz, 1H), 7.98 (d,  $J = 7.6$  Hz, 2H), 7.95–7.89 (m, 3H), 7.87 (d,  $J = 8.2$  Hz, 1H), 7.77 (t,  $J = 7.8$  Hz, 1H), 7.70 (d,  $J = 8.1$  Hz, 1H), 7.66 (d,  $J = 8.1$  Hz, 1H), 7.62 (t,  $J = 7.8$  Hz, 1H), 7.46–7.38 (m, 3H), 7.31 (t,  $J = 7.7$  Hz, 2H), 7.17 (dd,  $J = 12.0, 7.0$  Hz, 2H), 7.14–7.05 (m, 3H), 6.77 (dd,  $J = 8.6, 6.7$  Hz, 2H), 6.66 (t,  $J = 6.5$  Hz, 1H), 6.50 (s, 1H), 6.27 (s, 1H).  $^{13}\text{C}$  NMR (75 MHz,  $\text{CDCl}_3$ )  $\delta$  206.90, 174.53, 166.77, 149.72, 149.31, 145.33, 143.80, 137.48, 137.05, 131.04, 130.92, 130.85, 130.76, 130.64, 129.16, 128.36, 128.19, 128.11, 127.95, 127.64, 123.34, 123.24, 122.74, 122.32, 119.03, 118.68, 118.11. HR EI-MS Calcd for  $[M + H]^+$ :  $m/z$  994.1415, found:  $m/z$  994.1415. Anal. calcd for  $\text{C}_{43}\text{H}_{27}\text{O}_2\text{N}_3\text{PF}_8\text{Ir}$ : C 52.02, N 4.23, H 2.74. Found: C 51.42, N 4.87, H 2.92.

**(tfmppy)<sub>2</sub>Ir(L3) (Ir3)**. 0.40 g  $[(\text{tfmppy})_2\text{Ir}(\mu\text{-Cl})_2]$  and 0.29 g **L3** gave 0.31 g **Ir3** (0.28 mmol, 46.7%).  $^1\text{H}$  NMR (500 MHz,  $\text{CDCl}_3$ )  $\delta$  9.17 (d,  $J = 5.6$  Hz, 1H), 8.31 (d,  $J = 5.6$  Hz, 1H), 8.10 (dd,  $J = 11.6, 8.2$  Hz, 2H), 8.02 (d,  $J = 7.3$  Hz, 2H), 7.93 (d,  $J = 8.1$  Hz, 1H), 7.86 (d,  $J = 8.1$  Hz, 1H), 7.79 (t,  $J = 7.8$  Hz, 1H), 7.74–7.64 (m, 4H), 7.59 (dd,  $J = 10.8, 8.4$  Hz, 2H), 7.54 (t,  $J = 7.8$  Hz, 1H), 7.45 (t,  $J = 7.4$  Hz, 1H), 7.34 (t,  $J = 7.7$  Hz, 4H), 7.20 (dd,  $J = 14.1, 7.1$  Hz, 2H), 7.14 (d,  $J = 8.0$  Hz, 1H), 6.55 (t,  $J = 6.6$  Hz, 1H), 6.52 (s, 1H), 6.25 (s, 1H).  $^{13}\text{C}$  NMR (75 MHz,  $\text{CDCl}_3$ )  $\delta$  206.90, 174.53, 166.77, 149.72, 149.31, 145.33, 143.80, 137.48, 137.05, 131.04, 130.92, 130.85, 130.76, 130.64, 129.16, 128.36, 128.19, 128.11, 127.95, 127.64, 123.34, 123.24, 122.74, 122.32, 119.03, 118.68, 118.11. HR EI-MS Calcd for  $[M + H]^+$ :  $m/z$  1094.1351, found:  $m/z$  1094.1351. Anal. calcd for  $\text{C}_{45}\text{H}_{27}\text{O}_2\text{N}_3\text{PF}_{12}\text{Ir}$ : C 49.45, N 3.84, H 2.49. Found: C 49.48, N 3.79, H 2.58.

**(tfmppy)<sub>2</sub>Ir(L4) (Ir4)**. 0.40 g  $[(\text{tfmppy})_2\text{Ir}(\mu\text{-Cl})_2]$  and 0.24 g **L4** gave 0.17 g **Ir4** (0.17 mmol, 42.9%).  $^1\text{H}$  NMR (500 MHz,  $\text{CDCl}_3$ )  $\delta$  9.19 (d,  $J = 5.6$  Hz, 1H), 8.28 (d,  $J = 5.6$  Hz, 1H), 7.92 (d,  $J = 8.1$  Hz, 1H), 7.90–7.83 (m, 3H), 7.79 (t,  $J = 7.8$  Hz, 1H), 7.70 (d,  $J = 8.1$  Hz, 1H), 7.66 (d,  $J = 8.1$  Hz, 1H), 7.64–7.53 (m, 3H), 7.50–7.35 (m, 5H), 7.30 (d,  $J = 10.3$  Hz, 2H), 7.22–7.16 (m, 1H), 7.15 (d,  $J = 5.4$  Hz, 1H), 7.13–7.10 (m, 2H), 6.60 (t,  $J = 6.6$  Hz, 1H), 6.50 (s, 1H), 6.26 (s, 1H).  $^{13}\text{C}$  NMR (75 MHz,  $\text{CDCl}_3$ )  $\delta$  206.90, 174.53, 166.77, 149.72, 149.31, 145.33, 143.80, 137.48, 137.05, 131.04, 130.92, 130.85, 130.76, 130.64, 129.16, 128.36, 128.19, 127.95, 127.64, 123.34, 123.24, 122.74, 122.32, 119.03, 118.68, 118.11. HR EI-MS Calcd for  $[M + H]^+$ :  $m/z$  1012.1321, found:  $m/z$  1012.1323. Anal. calcd for  $\text{C}_{43}\text{H}_{26}\text{O}_2\text{N}_3\text{PF}_9\text{Ir}$ : C 51.09, N 4.16, H 2.59. Found: C 51.30, N 3.89, H 2.31.

**(tfmppy)<sub>2</sub>Ir(L5) (Ir5)**. 0.40 g  $[(\text{tfmppy})_2\text{Ir}(\mu\text{-Cl})_2]$  and 0.22 g **L5** gave 0.14 g **Ir5** (0.15 mmol, 74.5%).  $^1\text{H}$  NMR (500 MHz,  $\text{CDCl}_3$ )  $\delta$  9.23 (d,  $J = 5.5$  Hz, 1H), 8.34 (d,  $J = 5.5$  Hz, 1H), 7.99 (dd,  $J = 8.0, 6.1$  Hz, 2H), 7.91 (t,  $J = 6.2$  Hz, 2H), 7.89 (s, 1H), 7.85 (d,  $J = 8.1$  Hz, 1H), 7.76 (t,  $J = 7.7$  Hz, 1H), 7.69 (d,  $J = 8.1$  Hz, 1H), 7.65 (d,  $J = 8.1$  Hz, 1H), 7.55 (t,  $J = 7.7$  Hz, 1H), 7.45 (s, 1H), 7.42 (dd,  $J = 10.9, 7.2$  Hz, 4H), 7.27 (d,  $J = 7.4$  Hz, 1H), 7.16 (t,  $J = 8.3$  Hz, 2H), 7.14–7.09 (m, 2H), 7.08 (d,  $J = 5.0$  Hz, 1H), 6.96 (t,  $J = 8.6$  Hz, 2H), 6.58 (t,  $J = 6.5$  Hz, 1H), 6.51 (s, 1H), 6.29 (s, 1H).  $^{13}\text{C}$  NMR (75 MHz,  $\text{CDCl}_3$ )  $\delta$  206.90, 174.53, 166.77, 149.72, 149.31, 145.33, 143.80, 137.48, 137.05, 131.04, 130.92, 130.85, 130.76, 130.64, 129.16, 128.36, 128.19, 128.11, 127.95, 127.64, 123.34, 123.24, 122.74, 122.32, 119.03, 118.68, 118.11. HR EI-MS Calcd for  $[M + H]^+$ :  $m/z$  976.1509, found:  $m/z$  976.1509. Anal. calcd for  $\text{C}_{43}\text{H}_{28}\text{O}_2\text{N}_3\text{PF}_{11}\text{Ir}$ : C 52.98, N 4.31, H 2.89. Found: C 53.01, N 4.39, H 2.63.

**(tfmppy)<sub>2</sub>Ir(L6) (Ir6)**. 0.40 g  $[(\text{tfmppy})_2\text{Ir}(\mu\text{-Cl})_2]$  and 0.26 g **L6** gave 0.14 g **Ir6** (0.13 mmol, 65.3%).  $^1\text{H}$  NMR (500 MHz,  $\text{CDCl}_3$ )  $\delta$  9.13 (d,  $J = 5.5$  Hz, 1H), 8.28 (d,  $J = 5.5$  Hz, 1H), 7.94 (d,  $J = 8.1$  Hz, 1H), 7.89 (d,  $J = 8.3$  Hz, 2H), 7.85 (d,  $J = 8.5$  Hz, 1H), 7.81 (t,  $J = 7.8$  Hz, 1H), 7.70 (d,  $J = 8.1$  Hz, 1H), 7.65 (dd,  $J = 15.9, 7.8$  Hz, 2H), 7.61–7.54 (m, 2H), 7.42–7.33 (m, 2H), 7.21 (t,  $J = 6.6$  Hz, 1H), 7.17 (d,  $J = 8.2$  Hz, 1H), 7.15 (s, 1H), 7.12 (d,  $J = 8.9$  Hz, 2H), 6.80 (t,  $J = 7.7$  Hz, 2H), 6.69 (t,  $J = 6.5$  Hz, 1H), 6.49 (s, 1H), 6.23 (s, 1H).  $^{13}\text{C}$  NMR (75 MHz,  $\text{CDCl}_3$ )  $\delta$  206.90, 174.53, 166.77, 149.72, 149.31, 145.33, 143.80, 137.48, 137.05, 131.04, 130.92, 130.85, 130.76, 130.64, 129.16, 128.36, 128.19, 128.11, 127.95, 127.64, 123.34, 123.24, 122.74, 122.32, 119.03, 118.68, 118.11. HR EI-MS Calcd for  $[M + H]^+$ :  $m/z$  1048.1132, found:  $m/z$  1048.1132. Anal. calcd for  $\text{C}_{43}\text{H}_{24}\text{O}_2\text{N}_3\text{PF}_{11}\text{Ir}$ : C 49.33, N 4.01, H 2.31. Found: C 49.32, N 4.08, H 2.52.

**(tfmppy)<sub>2</sub>Ir(L7) (Ir7)**. 0.40 g  $[(\text{tfmppy})_2\text{Ir}(\mu\text{-Cl})_2]$  and 0.24 g **L7** gave 0.09 g **Ir7** (0.09 mmol, 43.1%).  $^1\text{H}$  NMR (500 MHz,  $\text{CDCl}_3$ )  $\delta$  9.16 (d,  $J = 5.6$  Hz, 1H), 8.34 (d,  $J = 5.6$  Hz, 1H), 8.01–7.94 (m, 2H), 7.91 (d,  $J = 8.0$  Hz, 2H), 7.88 (d,  $J = 7.5$  Hz, 2H), 7.78 (t,  $J = 7.8$  Hz, 1H), 7.70 (d,  $J = 8.1$  Hz, 1H), 7.64 (dd,  $J = 18.1, 8.1$  Hz, 2H), 7.44–7.35 (m, 2H), 7.19 (d,  $J = 7.0$  Hz, 1H), 7.16 (d,  $J = 8.6$  Hz, 1H), 7.13 (s, 1H), 7.12–7.06 (m, 2H), 6.96 (t,  $J = 8.6$  Hz, 2H), 6.78 (t,  $J = 7.9$  Hz, 2H), 6.67 (t,  $J = 6.5$  Hz, 1H), 6.50 (s, 1H), 6.26 (s, 1H).  $^{13}\text{C}$  NMR (75 MHz,  $\text{CDCl}_3$ )  $\delta$  206.90, 174.53, 166.77, 149.72, 149.31, 145.33, 143.80, 137.48, 137.05, 131.04, 130.92, 130.85, 130.76, 130.64, 129.16, 128.36, 128.19, 128.11, 127.95, 127.64, 123.34, 123.24, 122.74, 122.32, 119.03, 118.68, 118.11. HR EI-MS Calcd for  $[M + H]^+$ :  $m/z$  1012.1321, found:  $m/z$  1012.1321. Anal. calcd for  $\text{C}_{43}\text{H}_{26}\text{O}_2\text{N}_3\text{PF}_9\text{Ir}$ : C 51.09, N 4.16, H 2.59. Found: C 50.89, N 4.22, H 2.73.

### 3. Results and discussion

#### 3.1. Syntheses and X-ray crystallography

Although the synthesis of **L1** has been reported [34], triethylamine, which is hard to dehydration, was required as a base in the reaction. Here we demonstrate that the 4-dimethylaminopyridine (DMAP) could also make the reaction efficient. The electron-

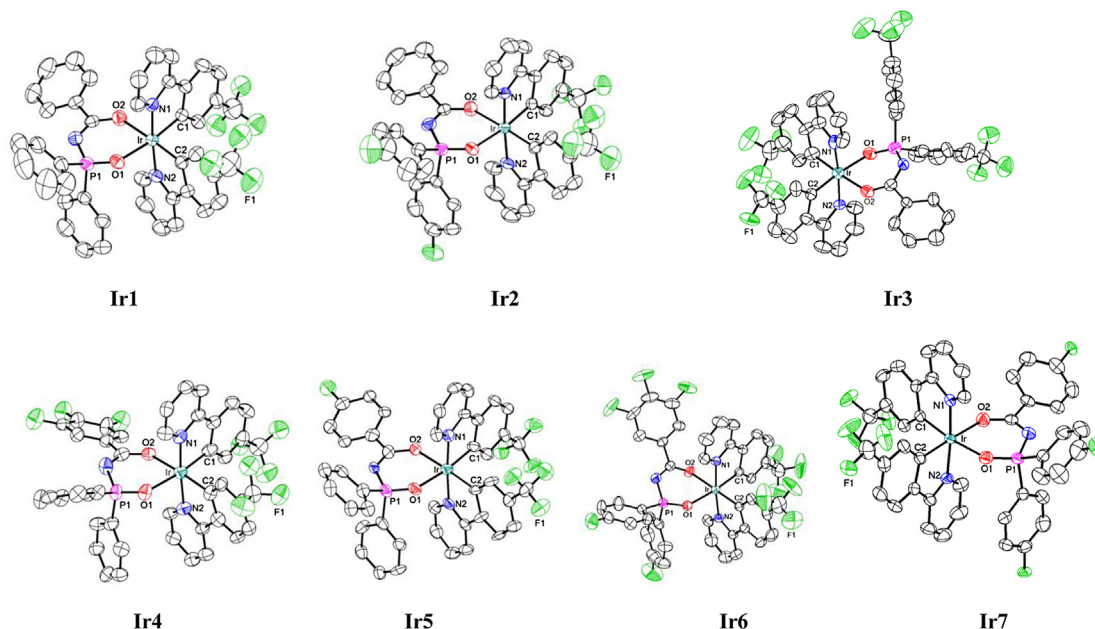


**Fig. 1.** Molecular structures of **Ir1–Ir7** with thermal ellipsoids shown at 50% probability level. The hydrogen atoms are omitted for clarity.

withdrawing fluorine and trifluoromethyl substituents were introduced in either or both benzamides and chlorodiphenylphosphines moieties, hoping to alter the energy levels of frontier molecular orbitals in the complexes and change the photophysical properties consequently.

The single crystals of **Ir1**, **Ir2**, **Ir3**, **Ir4**, **Ir5**, **Ir6** and **Ir7** were obtained by using solvent diffusion of MeOH into CH<sub>2</sub>Cl<sub>2</sub> solutions of the complexes at room temperature. The Oak Ridge thermal ellipsoidal plot (ORTEP) diagrams of the complexes are shown in Fig. 1. The parameters of the refined single crystals are selected in Table 1. Important bond lengths and angles revealing the coordination sphere are listed in Table S1 as Supporting information.

The single crystal structure diagrams in Fig. 1 reveal that each complex possesses the pseudo-octahedral coordination geometry, which is typical for heteroleptic iridium complexes. The relative coordination geometry of the cyclometallated phenylpyridine ligands is retained from that of the precursors with *cis*-C,C and *trans*-

*N,N* coordination and the chelated *N*-(diphenylphosphoryl)benzamide derivatives bond through oxygen donor atoms. From a steric perspective it is noted that one of the phenyl moieties attached to phosphorus atom is bent into a parallel position with the pyridine moiety in phenylpyridine ligand in an effort to minimize the interactions caused by sterically crowded diphenylphosphoryl moiety. As a result of this packing effect, the hexatomic-ring coordination structure of ancillary ligand and iridium center is disturbed. The phosphorus atom is obviously drawn along with the packing phenyl moiety, as well as the conjoint nitrogen and oxygen atoms.

Among all the coordination bonds, the Ir–O bonds are the longest (2.151–2.246 Å). It is not surprising to find that the Ir–C bonds (1.965–2.025 Å) are shorter than Ir–N bonds (2.028–2.049 Å) in each complex, suggesting the stronger coordination effect of Ir–C bonds than Ir–N bonds. Consequently, the N(1)–Ir–N(2) bond angles are twisted slightly, ranging from 174.18° to

**Table 1**

Parameters associated with the single crystal diffraction data collection for **Ir1**, **Ir2**, **Ir3**, **Ir4**, **Ir5**, **Ir6** and **Ir7**.

	<b>Ir1</b>	<b>Ir2</b>	<b>Ir3</b>	<b>Ir4</b>	<b>Ir5</b>	<b>Ir6</b>	<b>Ir7</b>
Formula	C <sub>43</sub> H <sub>29</sub> F <sub>6</sub> IrN <sub>3</sub> O <sub>2</sub> P	C <sub>43</sub> H <sub>27</sub> F <sub>8</sub> IrN <sub>3</sub> O <sub>2</sub> P	C <sub>45</sub> H <sub>27</sub> F <sub>12</sub> IrN <sub>3</sub> O <sub>2</sub> P	C <sub>43</sub> H <sub>26</sub> F <sub>9</sub> IrN <sub>3</sub> O <sub>2</sub> P	C <sub>43</sub> H <sub>28</sub> F <sub>7</sub> IrN <sub>3</sub> O <sub>2</sub> P	C <sub>43</sub> H <sub>24</sub> F <sub>11</sub> IrN <sub>3</sub> O <sub>2</sub> P	C <sub>43</sub> H <sub>26</sub> F <sub>9</sub> IrN <sub>3</sub> O <sub>2</sub> P
Formula weight	956.88	992.85	1092.87	1010.84	974.85	1046.84	1010.86
Crystal system	Monoclinic	Monoclinic	Monoclinic	Triclinic	Monoclinic	Monoclinic	Monoclinic
Space group	<i>P2</i> <sub>1</sub> / <i>n</i>	<i>P2</i> <sub>1</sub> / <i>n</i>	<i>P2</i> <sub>1</sub> / <i>c</i>	<i>P1</i>	<i>P2</i> <sub>1</sub> / <i>n</i>	<i>P2</i> <sub>1</sub> / <i>n</i>	<i>P2</i> <sub>1</sub> / <i>n</i>
<i>a</i> [Å]	13.3295(4)	13.3226(10)	14.4337(8)	11.956(3)	13.364(11)	10.1550(7)	13.1209(11)
<i>b</i> [Å]	19.9555(6)	19.7284(15)	23.7048(13)	12.148(4)	20.114(17)	15.8578(11)	19.4821(16)
<i>c</i> [Å]	14.2885(4)	14.5722(11)	13.7494(7)	15.466(5)	14.351(12)	24.4654(17)	14.4441(12)
$\alpha$ [°]	90	90	90	96.493(4)	90	90	90
$\beta$ [°]	97.1550(10)	96.3670(10)	111.913(2)	102.451(4)	96.892(12)	96.5590(10)	95.8500(10)
$\gamma$ [°]	90	90	90	115.984(3)	90	90	90
<i>V</i> [Å <sup>3</sup> ]	3771.10(19)	3806.4(5)	4364.4(4)	1915.8(10)	3830(6)	3914.0(5)	3673.0(5)
<i>Z</i>	4	4	4	2	4	4	4
<i>F</i> (000)	1880	1944	2136	988	1912	2040	1976
Reflns collected	25,495	34,050	34,728	15,374	19,713	32,962	32,626
Unique( <i>R</i> <sub>int</sub> )	8653(0.0208)	8725(0.0491)	8546(0.0118)	7427(0.0203)	6562(0.0414)	8539(0.0922)	8394(0.0449)
<i>R</i> <sub>1</sub> , <i>wR</i> <sub>2</sub> [ <i>I</i> > 2σ( <i>I</i> )]	0.0276, 0.0688	0.0331, 0.0876	0.0595, 0.1469	0.0594, 0.1463	0.0478, 0.1115	0.0409, 0.0971	0.0287, 0.0716
<i>R</i> <sub>1</sub> , <i>wR</i> <sub>2</sub> [all data]	0.0351, 0.0724	0.0420, 0.0976	0.0633, 0.1477	0.0620, 0.1473	0.0548, 0.1125	0.0627, 0.1082	0.0388, 0.0768
GO F [F <sup>2</sup> ]	1.033	1.068	1.039	1.010	1.033	1.016	1.075
CCDC number	930983	930984	930985	930986	930987	930988	930989

$$R_1 = \frac{\sum ||F_o| - |F_c||}{\sum |F_o|}, wR_2 = \frac{[\sum w(F_o^2 - F_c^2)^2]}{\sum w(F_o^2)^2}^{1/2}.$$

175.70°. Concerning the bond angles between the two phenyl moieties and phosphorus atom, since one of the phenyl rings is almost fixed in the parallel position with the pyridine ring, the other automatically adjust a most favorable structure which forms a flare angle around 109°.

### 3.2. Electrochemistry

The electrochemical behaviors of these iridium complexes were investigated by cyclic voltammetry in deaerated acetonitrile in order to determine the HOMO/LUMO energy levels ( $E_{\text{HOMO}}/E_{\text{LUMO}}$ ). The ionization potential for the first oxidation ( $\text{Ir}^{\text{III/IV}}$ ) can be used to establish  $E_{\text{HOMO}}$  by assuming that the absolute level of the  $\text{Fc}^{\text{0/I}}$  redox couple is 4.8 eV below the vacuum level, and further LUMO energy levels can be calculated from the HOMOs and energy bandgaps obtained from the lowest-energy absorption edges of the UV–vis spectra. The cyclic voltammograms of the complexes **Ir1**–**Ir7** ( $5 \times 10^{-4}$  M) solutions show distinct reversible redox peaks and the oxidation peaks are in the region of 1.00–1.05 V (Fig. 2). These positive oxidation potentials are attributed to the center  $\text{Ir}^{\text{III/IV}}$  oxidations, in accordance with the reported cyclometallated  $\text{Ir}^{\text{III}}$  systems.

Although the differences among oxidation potentials are not obvious, the electron-withdrawing  $-\text{CF}_3$  and  $-\text{F}$  substituents on the ancillary ligands led to certain anodic shift of the oxidation potential. This is demonstrated by the oxidation potential sequences of **Ir3** (1.053 V) > **Ir2** (1.014 V) > **Ir1** (0.997 V), and **Ir6** (1.049 V) > **Ir4** (1.031 V) > **Ir7** (1.022 V) > **Ir5** (1.004 V) > **Ir1** (0.997 V). Meanwhile, from the sequences of the oxidation peaks, it can be concluded that the amount of the substituents in the ancillary ligands have predominant influences and the electron-withdrawing unit of  $-\text{CF}_3$  has a little effect than that of F. Consequently, the HOMO resultant values (Table 2), using the reported equations [24,35], range from  $-5.53$  to  $-5.58$  eV for complexes **Ir1**–**Ir7**. The introduction of the electron-withdrawing moieties of  $-\text{CF}_3$  and F can decrease the HOMO energy levels. Specifically, for the complex **Ir3** with  $-\text{CF}_3$  substituents, the HOMO values are  $-5.58$  eV and for complexes **Ir6**, **Ir4**, **Ir7**, **Ir2** and **Ir5** with F atoms, the HOMO data are  $-5.57$ ,  $-5.56$ ,  $-5.55$ ,  $-5.54$  and  $-5.53$  eV, respectively.

### 3.3. Density function theory (DFT) study

In an effort to elucidate the nature of the electronic transitions within this series of complexes, DFT calculations (computed using

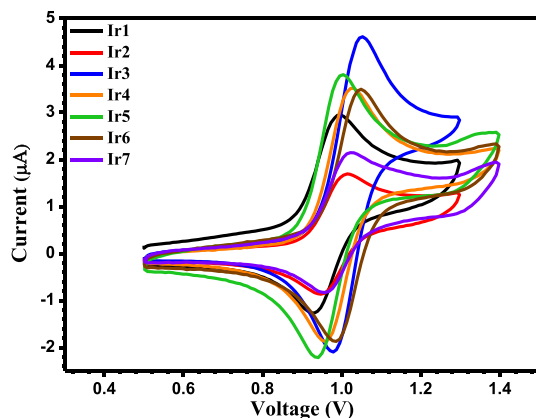


Fig. 2. Cyclic voltammograms of the complexes **Ir1**–**Ir7**.

**Table 2**  
Electrochemical data of the complexes **Ir1**–**Ir7**.

Complex	$E_{\text{ox}}/\text{V}^{\text{a}}$	$E_{\text{red}}/\text{V}^{\text{a}}$	$E_{\text{HOMO}}/\text{eV}^{\text{b}}$	$E_{\text{bandgap}}/\text{eV}^{\text{c}}$	$E_{\text{LUMO}}/\text{eV}^{\text{d}}$
<b>Ir1</b>	+0.997	+0.931	−5.53	2.47	−3.06
<b>Ir2</b>	+1.014	+0.947	−5.54	2.51	−3.03
<b>Ir3</b>	+1.053	+0.979	−5.58	2.53	−3.05
<b>Ir4</b>	+1.031	+0.959	−5.56	2.61	−2.95
<b>Ir5</b>	+1.004	+0.941	−5.53	2.57	−2.96
<b>Ir6</b>	+1.049	+0.986	−5.57	2.58	−2.99
<b>Ir7</b>	+1.022	+0.959	−5.55	2.56	−2.99

<sup>a</sup> Oxidation potentials measured as MeCN solutions at  $50 \text{ mV s}^{-1}$  with  $0.10 \text{ M}$   $\text{Bu}_4\text{NClO}_4$  as supporting electrolyte calibrated with ferrocene.

<sup>b</sup> The HOMO energy levels were calculated using the equation  $-\text{HOMO} (\text{eV}) = E_{\text{ox}} - E_{\text{Fc}/\text{Fc}^+} + 4.8$ .

<sup>c</sup>  $E_{\text{bandgap}}$  energies were determined from the absorption edge of the iridium complexes.

<sup>d</sup> The LUMO energy levels were calculated using the equation  $\text{LUMO} (\text{eV}) = \text{HOMO} + E_{\text{bandgap}}$ .

the B3LYP hybrid functional) were undertaken. The resultant assessment of the frontier orbitals provides a qualitative insight into the HOMO and LUMO energy levels. Contour plots of the frontier molecular orbitals (FMOs) are shown in Fig. 3, while the energies and descriptions of them, in terms of % composition of ligand and metal orbitals, are collected in Table 3. The detailed information for other frontier molecular orbitals of all the complexes is given in Table S2 as Supporting information.

From the point of view of the electronic structure, all the complex models display the typical features of complexes containing iridium atom in a pseudo-octahedral coordination sphere. In detail, the three highest occupied orbitals (HOMO, HOMO  $- 1$  and HOMO  $- 2$ ) are mainly localized on the iridium atom while the lowest unoccupied molecular orbitals are mainly localized on the  $\pi$  orbitals of phenylpyridine ligands. Population analyses (Table 3) reveal that the distributions of the FMOs for all the complexes have similar electron distributions on HOMOs and LUMOs. Specifically, HOMOs consists of the  $d$  orbital (54.2–54.5%) of iridium atom and  $\pi$  orbitals (37.8–38.5%) of  $\text{tfmppy}$ , indicating substantial mixing of the  $\pi$  orbitals of the ligands with the metal. HOMO  $- 1$  and HOMO  $- 2$  are near-degenerate (energy difference is in the range of 0.02–0.03 eV), and share the similar contributions from mostly iridium  $d$  orbital (>60%) together with  $\pi$  orbitals of both ligands. The LUMO and LUMO  $+ 1$  are both predominantly located on the  $\pi$  orbitals (92.4–94.1%) of  $\text{tfmppy}$ . The almost degenerated couple of LUMO and LUMO  $+ 1$  are favorable for the stabilization of excited electrons, which makes the complexes have better capability in holding the excited electrons, and benefits electron transportation process [36]. It is worthy to mention that most  $\pi$  orbital contributions from  $\text{tfmppy}$  on HOMOs are localized on the phenyl and the contribution from the pyridine rings is negligible. But for LUMOs, phenyl and pyridine rings share almost the equal contributions. This provides a possible molecular design strategy for such iridium complexes with phenylpyridine ligands that electron-donating and electron-withdrawing substituents can be attached to the phenyl rings to alter HOMO energy levels, and LUMO energy levels can be altered efficiently when attached the substituents to the pyridine rings. Meanwhile, according to previous reports, the quantum efficiency values of the phosphorescence emission of the iridium complexes could be kept on a quite high level, since the LUMOs are dominantly contributed by main ligands [37,38], and the following experimental data prove this presumption.

Since the ancillary ligands have little contributions on HOMOs (7.0–7.7%) and LUMOs (2.1–3.6%), it is not surprising that with the change of the ancillary ligands, the energy levels of both HOMOs and LUMOs do not have significant differences. As a result, the HOMO–LUMO energy gaps are similar, and this can explain that the

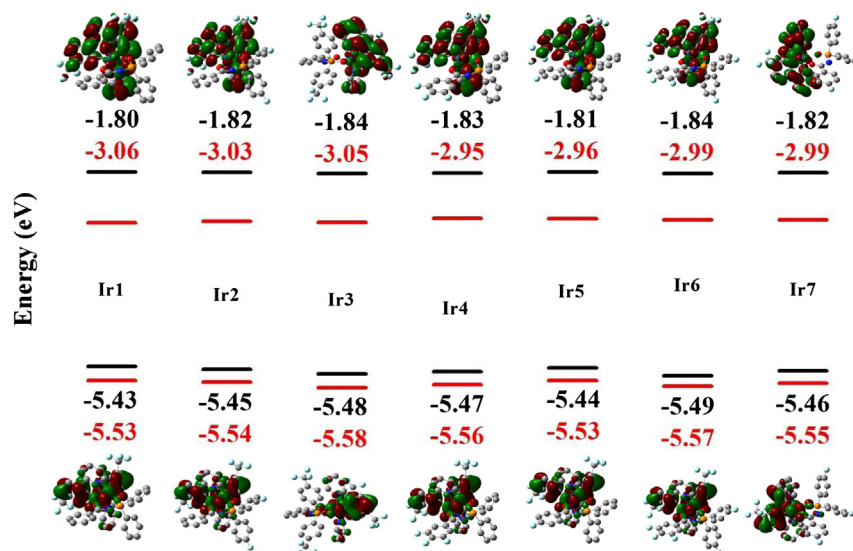


**Fig. 3.** Contour plots of HOMOs (bottom) and LUMOs (top) of **Ir1–Ir7** with theoretical (black) and experimental (red, determined by cyclic voltammetry) energy levels. (For interpretation of the references to colour in this figure legend, the reader is referred to the web version of this article.)

emission peaks of the complexes are all around 520 nm. However, with the same tfmpppy main ligand, the subtle variations on the energy levels of FMOs can be ascribed to the electron-withdrawing  $-F$  or  $-CF_3$  substitutes attached to the ancillary ligands. Definitely, due to the relativistic effects, absolute energy levels cannot be reliably calculated for complexes of heavy metal ions, but relative energy levels can still be informative. For example, **Ir3** with a  $-CF_3$  substitutes on ancillary ligand has the lowest HOMO and LUMO energy levels ( $-5.58$  and  $-3.05$  eV, respectively). For **Ir5**, **Ir4**, **Ir7** and **Ir6**, with the increase of fluorine atom number on ancillary ligands, the HOMO levels decrease consequently ( $-5.44 > -5.47 \approx -5.46 > -5.49$  eV) and this sequence coincides with the experimental data ( $-5.53 > -5.56 \approx -5.55 > -5.57$  eV).

When compared the theoretical calculated energy levels with the experimental data, HOMO energy levels are in good agreement with the experimental ones and the difference is around 0.1 eV. However, for LUMO energy levels, the calculated results are about 1.2 eV lower than experimental values. These differences simply reflect the ignorance of relaxation effects, which may lower the LUMO energies in great deal, during the theoretical calculation [39], because the calculated values are approximations to vertical oxidation/reduction potentials.

**Table 3**  
Percentage distributions of HOMO and LUMO in the complexes **Ir1–Ir7**.

Complex	Orbital	Energy/eV	$E_{bandgap}/eV$	Composition %		
				Ir	L	tfmpppy
<b>Ir1</b>	HOMO	-5.43	3.63	54.5	7.7	37.8
	LUMO	-1.80		3.9	2.1	94.1
<b>Ir2</b>	HOMO	-5.45	3.63	54.2	7.5	38.3
	LUMO	-1.82		3.9	2.2	94.0
<b>Ir3</b>	HOMO	-5.48	3.64	54.4	7.2	38.1
	LUMO	-1.84		3.9	3.6	92.4
<b>Ir4</b>	HOMO	-5.47	3.64	54.4	7.3	38.3
	LUMO	-1.83		3.9	2.3	93.8
<b>Ir5</b>	HOMO	-5.44	3.63	54.4	7.6	37.9
	LUMO	-1.81		3.9	2.1	94.1
<b>Ir6</b>	HOMO	-5.49	3.65	54.5	7.0	38.5
	LUMO	-1.84		3.9	2.2	93.9
<b>Ir7</b>	HOMO	-5.46	3.64	54.4	7.5	38.2
	LUMO	-1.82		3.9	2.1	94.0

### 3.4. Photophysical property

The UV–vis absorption spectra of the complexes were measured in aerated  $CH_2Cl_2$  solutions (Fig. 4(a), Table 4). The intense bands, which observed in the ultraviolet part of the spectra, between 220 and 280 nm ( $\epsilon > 10^4 M^{-1} cm^{-1}$ ), can be assigned safely to the spin-allowed  $^1\pi-\pi^*$  transition of the ligand-centered ( $^1LC$ ) states. In the range of lower energy ( $300 < \lambda < 525$  nm), the absorption spectra show subtle variations and can be assigned to singlet and triplet MLCT transitions and ligand-to-ligand charge transfers [40–43], suggesting that the electronic structures of the frontier orbitals are almost the same in all the complexes, which has been proved by earlier DFT studies.

Time-dependent DFT (TD-DFT) calculations in simulated  $CH_2Cl_2$  on all the complexes well support the assignment of these bands. It is noteworthy that compared with B3LYP functional, M06-2x functional reproduces the absorption spectra profiles that match the experimental data better, especially in the high-energy range. The absorption energies with large oscillator strength, their dominant configurations and transition nature are listed in Table S3 and the simulated spectra are depicted in Fig. S1. To facilitate the comparison, a broadening of the transition with  $FWHM = 5000 cm^{-1}$  is applied to all calculated spectra. Taking **Ir1** as example to discuss in detail (Fig. 4(b)), generally, a reasonable agreement is obtained between the theoretical and experimental spectra. The lowest-energy absorption with significant intensity consists of excitation from the HOMO that localized on  $5d$  orbital of iridium (54.5%) and  $\pi$  orbital of tfmpppy (37.8%) into LUMO dominated by  $\pi^*$  orbitals of tfmpppy (94.1%). This transition is predicted to lie at 339 nm (oscillator strength = 0.13 a.u.) which is in good agreement with the energy gap ( $\Delta E_{HOMO-LUMO}$ ), and possesses the nature of MLCT. Since only singlet–singlet transitions are taken into consideration during the calculations, and there is no absorption band in the range from 400 to 500 nm in the simulated spectrum. Thus, the weak absorption in this range in the experimental spectrum can be assigned to spin-forbidden triplet metal-to-ligand charge-transfer ( $^3MLCT$ ) transitions and  $^3\pi-\pi^*$  transitions of the ligands ( $d\pi-\pi^*$ ). A set of stronger transitions centered at around 260 nm (251 nm, 0.15 a.u.; 264 nm, 0.27 a.u.; 266 nm, 0.10 a.u.) are also predicted, in good agreement with experimental shoulder peaks. These bands consist of varying combinations of iridium

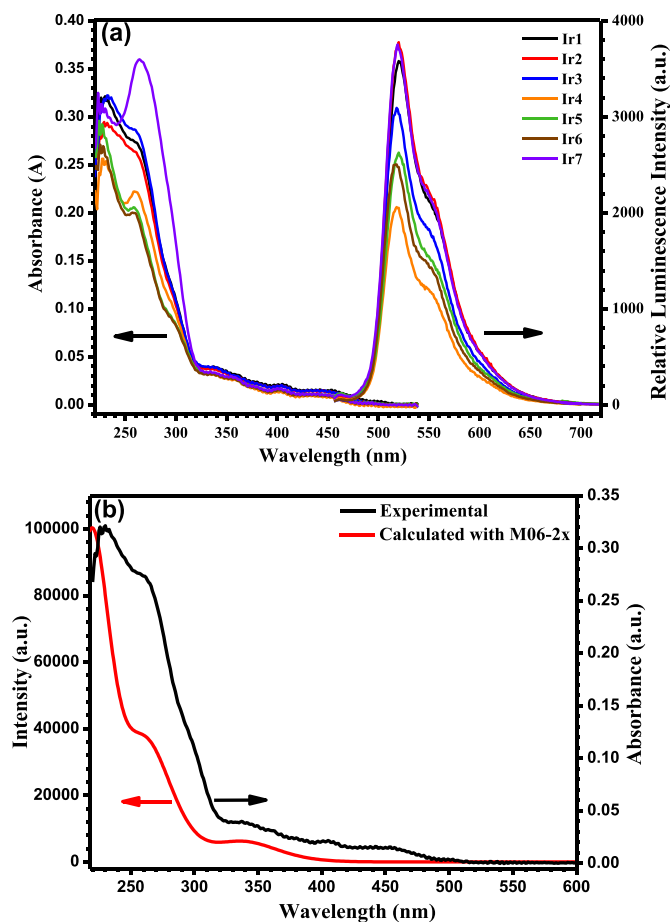


**Fig. 4.** (a) Absorption/emission spectra of **Ir1–Ir7** in aerated/deaerated  $\text{CH}_2\text{Cl}_2$  solutions. ( $5.0 \times 10^{-6}$  M for absorption spectra and  $5.0 \times 10^{-5}$  M for emission spectra); (b) Experimental spectrum (black) and theoretically simulated absorption spectrum (red) of **Ir1** in  $\text{CH}_2\text{Cl}_2$ . (For interpretation of the references to color in this figure legend, the reader is referred to the web version of this article.)

*d* orbitals, tfmpppy and part of **L1**  $\pi$  orbitals excited into tfmpppy  $\pi^*$  orbitals, suggesting contributions of MLCT and LLCT. The largest intensity bands include excitations from iridium *d* orbitals and  $\pi$  orbitals of both tfmpppy and **L1** into  $\pi^*$  orbitals of tfmpppy and **L1**, indicating ILCT and LLCT mixed with part of MLCT character.

Photoluminescence measurements were conducted in deaerated  $\text{CH}_2\text{Cl}_2$  solutions at room temperature (Fig. 4(a), Table 4) and

77 K (Fig. 5(a), Table 4). Emission spectra at room temperature (Fig. 4(a), left) show the broad and structured emission maxima at about 520 nm together with a shoulder peak at 560 nm. The emission peaks are very close to that of the  $\text{Ir}(\text{tfmpppy})_2(\text{acac})$  (522 nm) [11], indicating that this new series of ancillary ligands do not affect the electronic structures of the frontier orbitals that engaged in the emission process significantly and the change of the ancillary ligand leads to a really subtle shift in the emission color. It is quite prominent to identify a vibrational sideband pattern for each complex in the room temperature emission spectrum, suggesting that the emissive state has emission characteristic of phosphorescence from a mixed-ligand-centered-MLCT (LC-MLCT) triplet state [44–46]. There is no evidence of any significant emission around absorption bands at higher energies, which indicates efficient inter-system crossing (ISC) from the high-energy electronic excited states to the emitting states in these complexes. Concerning the photoluminescent efficiency, complexes **Ir2** and **Ir7** have relatively higher quantum yields of 61.2% and 58.2% than the **Ir1** (57.2%), which has no  $-\text{F}$  and  $-\text{CF}_3$  substituents in the ancillary ligand. However, **Ir3**, **Ir4**, **Ir5** and **Ir6** own relatively lower quantum yields of 46.8%, 37.5%, 47.8% and 47.4%, respectively, but still comparable to the efficiency of *fac*- $\text{Ir}(\text{ppy})_3$  standard reference. The sequence is well agreed with the emission intensities listed in Fig. 4(a). This proves that the non-radiative energy decay paths of most complexes are well depressed.

Emission spectra at 77 K (Fig. 5(a)) are divided into two main emission peaks which locate in the range from 513 to 516 nm and from 544 to 555 nm, respectively. This again demonstrates that the mixed  $^3\text{MLCT}$  and  $^3\text{LC}$  character of the emissive states of the complexes. As shown in Fig. 5(a) and Table 4, the phosphorescence spectra of the  $\text{Ir}^{\text{III}}$  complexes suffer the rigidochromic effect on going from fluid to glassy solvent: the phosphorescence bands shift to blue on going from RT to 77 K. The rigidochromic effect on some kinds of transition metal complexes has been previously reported [47,48]. This behavior usually indicates that the luminescent excited state is coupled with nuclear rearrangements which are affected by the state of the solvent. Because of the low viscosity of the medium at RT, solvent molecules in the vicinity of the excited-state molecule readily undergo reorientation by the dipole–dipole interaction within the lifetime of the excited state, resulting in the formation of the fully relaxed excited state. Thus, the emission at room temperature occurs from the fully relaxed excited state. On the other hand, the excited state at 77 K emits before the solvent relaxation occurs, resulting in the rigidochromic effects on the emission spectra. For solid state emissions at room temperature (Fig. 5(b)), all the complexes exhibit emission peaks in the range from 544 to 553 nm, which are substantially red-shifted from their

**Table 4**  
Absorption and emission data of the complexes **Ir1–Ir7**.

Complex	Absorption <sup>a</sup> $\lambda_{\text{max}}/\text{nm}$ ( $\epsilon/10^3 \text{ M}^{-1} \text{ cm}^{-1}$ )	Emission				
		Solution			Solid	
		$\lambda_{\text{em}}^{\text{RT}}/\text{nm}^{\text{b}}$	$\tau/\mu\text{s}^{\text{b}}$	$\Phi_{\text{em}}/\%^{\text{c}}$	$\lambda_{\text{em}}^{77\text{K}}/\text{nm}^{\text{d}}$	$\lambda_{\text{em}}/\text{nm}$ $\tau/\mu\text{s}$
<b>Ir1</b>	230 (64.2), 260 (54.8)sh, 337 (8.0), 404 (4.2), 442 (3.2)	521	2.0	57.2	514, 552	553 2.0
<b>Ir2</b>	229 (59.0), 260 (52.7)sh, 336 (7.5), 404 (4.0), 445 (3.0)	520	2.0	61.2	513, 545	548 2.4
<b>Ir3</b>	232 (64.4), 259 (57.4)sh, 336 (8.0), 404 (4.0), 440 (3.0)	518	1.9	46.8	515, 552	550 2.3
<b>Ir4</b>	228 (51.4), 259 (44.4), 337 (6.4), 403 (2.8), 442 (1.9)	518	2.1	37.5	514, 553	548 2.3
<b>Ir5</b>	225 (59.2), 258 (41.2), 295 (18.6)sh, 332 (6.7), 403 (3.3), 440 (2.2)	519	2.3	47.8	516, 554	549 2.6
<b>Ir6</b>	227 (54.2), 257 (40.0), 294 (18.4)sh, 337 (6.4), 401 (3.1), 437 (2.2)	517	2.1	47.4	515, 552	544 2.7
<b>Ir7</b>	226 (62.4), 264 (71.8), 334 (7.0)W, 402 (3.5), 440 (2.3)	520	2.0	58.2	516, 555	549 2.1

<sup>a</sup> Values were obtained from  $\text{CH}_2\text{Cl}_2$  solutions ( $5 \times 10^{-6}$  mol  $\text{L}^{-1}$ ) at room temperature, sh is marked as shoulder peak.

<sup>b</sup> Data were collected from deaerated  $\text{CH}_2\text{Cl}_2$  solutions ( $5 \times 10^{-4}$  mol  $\text{L}^{-1}$ ) at room temperature.

<sup>c</sup> Quantum efficiencies were calculated using *fac*- $\text{Ir}(\text{ppy})_3$  ( $\Phi_{\text{ref}} = 40\%$ ) in acetonitrile as reference.

<sup>d</sup> Data were collected from deaerated  $\text{CH}_2\text{Cl}_2$  solutions ( $5 \times 10^{-4}$  mol  $\text{L}^{-1}$ ) at 77 K.

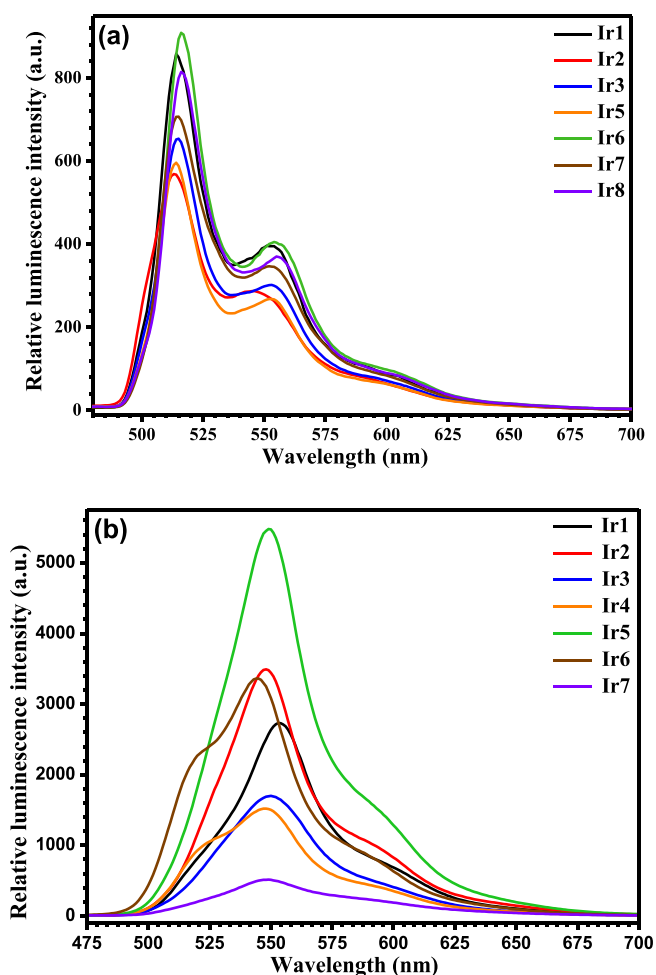


Fig. 5. The emission spectra for Ir1–Ir7 in deaerated  $\text{CH}_2\text{Cl}_2$  ( $5.0 \times 10^{-5}$  M) at 77 K (a) and solid state (b).

corresponding solution emissions (517–521 nm). These low-energy emissions can be ascribed to excimer formation arising from  $\pi$ – $\pi$  stacking interactions in the solid state, which will lead to a broad and featureless red-shifted luminescence compared with that in dilute solution [10,49].

As we know, the phosphorescence lifetime ( $\tau_p$ ) is the crucial factor that determines the rate of triplet–triplet annihilation in the OLEDs. The longer  $\tau_p$  of the material usually causes the more severe triplet–triplet annihilation [50,51]. The lifetimes of complexes are in the range of microseconds in  $\text{CH}_2\text{Cl}_2$  solution (1.9–2.3  $\mu\text{s}$ ) and in solid state (2.0–2.7  $\mu\text{s}$ ) at room temperature (Table 4, Figs. S2 and S3), which are indicative of the phosphorescent origin for the excited states in each case.

#### 4. Conclusion

We reported the syntheses and characterization of a series of new heteroleptic, phosphorescently emissive iridium complexes with *N*-(diphenylphosphoryl)benzamide derivatives as ancillary ligands. The molecular structures of the complexes reveal that each complex possesses pseudo-octahedral coordination geometry. The relative coordination geometry of the cyclometallated phenylpyridine ligands is retained from that of the precursors with *cis*-C,C and *trans*-N,N coordination and the chelated *N*-(diphenylphosphoryl)benzamide derivatives bond through oxygen donor atoms.

The electrochemical investigation and DFT calculation suggested that the –F and –CF<sub>3</sub> substituents on the ancillary ligands led to the anodic shift of the oxidation potential and decrease the HOMO energy levels. All the complexes own the similar emission peaks around 520 nm with various intensities and quantum efficiencies from 37.5 to 61.2% which suggesting the potential as phosphorescence dopants in the OLEDs. A wide range of substituents, electron-donating or -withdrawing units, can be attached to this kind of ligands in this way to obtain some promising complexes with attractive emissive properties.

#### Acknowledgments

This work was supported by the Major State Basic Research Development Program (2013CB922101, 2011CB808704) and the National Natural Science Foundation of China (21371093).

#### Appendix A. Supplementary material

CCDC 930983, 930984, 930985, 930986, 930987 and 930988 contain the supplementary crystallographic data for this paper. These data can be obtained free of charge from The Cambridge Crystallographic Data Centre via [www.ccdc.cam.ac.uk/data\\_request/cif](http://www.ccdc.cam.ac.uk/data_request/cif).

#### Appendix B. Supplementary data

Supplementary data related to this article can be found at <http://dx.doi.org/10.1016/j.jorganchem.2014.01.014>.

#### References

- [1] E.O. Danilov, I.E. Pomestchenko, S. Kinayyigit, P.L. Gentili, M. Hissler, R. Ziesler, F.N. Castellano, *J. Phys. Chem. A* 109 (2005) 2465.
- [2] S. Lamansky, P. Djurovich, D. Murphy, F. Abdel-Razzaq, H.E. Lee, C. Adachi, P.E. Burrows, S.R. Forrest, M.E. Thompson, *J. Am. Chem. Soc.* 123 (2001) 4304.
- [3] S. Sato, T. Morikawa, T. Kajino, O. Ishitani, *Angew. Chem. Int. Ed.* 52 (2013) 988.
- [4] J.A. Huang, J.S. Yu, Z.Q. Guan, Y.D. Jiang, *Appl. Phys. Lett.* 97 (2010) 143301.
- [5] Y. Tang, H.R. Yang, H.B. Sun, S.J. Liu, J.X. Wang, Q. Zhao, X.M. Liu, W.J. Xu, S.B. Li, W. Huang, *Chem. Eur. J.* 19 (2013) 1311.
- [6] M.A. Baldo, D.F. O'Brien, Y. You, A. Shoustikov, S. Sibley, M.E. Thompson, S.R. Forrest, *Nature* 395 (1998) 151.
- [7] E. Holder, B.M.W. Langeveld, U.S. Schubert, *Adv. Mater.* 17 (2005) 1109.
- [8] M.C. Gather, A. Kohnen, K. Meerholz, *Adv. Mater.* 23 (2011) 233.
- [9] F. Kessler, Y. Watanabe, H. Sasabe, H. Katagiri, M.K. Nazeeruddin, M. Gratzel, J. Kido, *J. Mater. Chem. C* 1 (2013) 1070.
- [10] S. Lamansky, P. Djurovich, D. Murphy, F. Abdel-Razzaq, R. Kwong, I. Tsyba, M. Bortz, B. Mui, R. Bau, M.E. Thompson, *Inorg. Chem.* 40 (2001) 1704.
- [11] Y.C. Zhu, L. Zhou, H.Y. Li, Q.L. Xu, M.Y. Teng, Y.X. Zheng, J.L. Zuo, H.J. Zhang, X.Z. You, *Adv. Mater.* 23 (2011) 4041.
- [12] M.Y. Teng, S. Zhang, S.W. Jiang, X. Yang, C. Lin, Y.X. Zheng, L. Wang, D. Wu, J.L. Zuo, X.Z. You, *Appl. Phys. Lett.* 100 (2012) 073303.
- [13] H.Y. Li, L. Zhou, M.Y. Teng, Q.L. Xu, C. Lin, Y.X. Zheng, J.L. Zuo, H.J. Zhang, X.Z. You, *J. Mater. Chem. C* 1 (2013) 560.
- [14] A. Juris, V. Balzani, F. Barigelletti, S. Campagna, P. Belser, A. Vonzelewsky, *Coord. Chem. Rev.* 84 (1988) 85.
- [15] M. Frank, M. Nieger, F. Vogtle, P. Belser, A. von Zelewsky, L. DeCola, V. Balzani, F. Barigelletti, L. Flamigni, *Inorg. Chim. Acta* 242 (1996) 281.
- [16] K.A. King, P.J. Spellane, R.J. Watts, *J. Am. Chem. Soc.* 107 (1985) 1431.
- [17] SAINT-Plus, Version 6.02, Bruker Analytical X-ray System, Madison, WI, 1999.
- [18] G.M. Sheldrick, SADABS An Empirical Absorption Correction Program, Bruker Analytical X-ray Systems, Madison, WI, 1996.
- [19] G.M. Sheldrick, SHELXTL-97, Universität of Göttingen, Göttingen, Germany, 1997.
- [20] E. Runge, E.K.U. Gross, *Phys. Rev. Lett.* 52 (1984) 997.
- [21] C.T. Lee, W.T. Yang, R.G. Parr, *Phys. Rev. B* 37 (1988) 785.
- [22] A.D. Becke, *J. Chem. Phys.* 98 (1993) 5648.
- [23] P.J. Hay, *J. Phys. Chem. A* 106 (2002) 1634.
- [24] B.W. D'Andrade, S. Datta, S.R. Forrest, P. Djurovich, E. Polikarpov, M.E. Thompson, *Org. Electron.* 6 (2005) 11.
- [25] X.N. Li, Z.J. Wu, Z.J. Si, H.J. Zhang, L. Zhou, X.J. Liu, *Inorg. Chem.* 48 (2009) 7740.
- [26] R.E. Strattmann, G.E. Scuseria, M.J. Frisch, *J. Chem. Phys.* 109 (1998) 8218.
- [27] N.N. Matsuzawa, A. Ishitani, D.A. Dixon, T. Uda, *J. Phys. Chem. A* 105 (2001) 4953.

- [28] Y. Zhao, D.G. Truhlar, *J. Phys. Chem. A* 110 (2006) 5121.
- [29] V. Barone, M. Cossi, *J. Phys. Chem. A* 102 (1998) 1995.
- [30] P.J. Hay, W.R. Wadt, *J. Chem. Phys.* 82 (1985) 299.
- [31] M.M. Francl, W.J. Pietro, W.J. Hehre, J.S. Binkley, M.S. Gordon, D.J. Defrees, J.A. Pople, *J. Chem. Phys.* 77 (1982) 3654.
- [32] M.J. Frisch, G.W. Trucks, H.B. Schlegel, G.E. Scuseria, M.A. Robb, J.R. Cheeseman, G. Scalmani, V. Barone, B. Mennucci, G.A. Petersson, H. Nakatsuji, M. Caricato, X. Li, H.P. Hratchian, A.F. Izmaylov, J. Bloino, G. Zheng, J.L. Sonnenberg, M. Hada, M. Ehara, K. Toyota, R. Fukuda, J. Hasegawa, M. Ishida, T. Nakajima, Y. Honda, O. Kitao, H. Nakai, T. Vreven, J.A. Montgomery Jr., J.E. Peralta, F. Ogliaro, M. Bearpark, J.J. Heyd, E. Brothers, K.N. Kudin, V.N. Staroverov, R. Kobayashi, J. Normand, K. Raghavachari, A. Rendell, J.C. Burant, S.S. Iyengar, J. Tomasi, M. Cossi, N. Rega, J.M. Millam, M. Klene, J.E. Knox, J.B. Cross, V. Bakken, C. Adamo, J. Jaramillo, R. Gomperts, R.E. Stratmann, O. Yazyev, A.J. Austin, R. Cammi, C. Pomelli, J.W. Ochterski, R.L. Martin, K. Morokuma, V.G. Zakrzewski, G.A. Voth, P. Salvador, J.J. Dannenberg, S. Dapprich, A.D. Daniels, O. Farkas, J.B. Foresman, J.V. Ortiz, J. Cioslowski, D.J. Fox, Gaussian 09, Revision A.01, Gaussian, Inc., Wallingford, CT, 2009.
- [33] N.M. O'Boyle, A.L. Tenderholt, K.M. Langner, *J. Comput. Chem.* 29 (2008) 839.
- [34] R. Garcia-Bueno, M.D. Santana, G. Sanchez, J. Garcia, G. Garcia, J. Perez, L. Garcia, *J. Organomet. Chem.* 694 (2009) 316.
- [35] A. Mishra, P.K. Nayak, D. Ray, M.P. Patankar, K.L. Narasimhan, N. Periasamy, *Tetrahedron Lett.* 47 (2006) 4715.
- [36] J. Wang, F.Q. Bai, B.H. Xia, H.X. Zhang, *J. Phys. Chem. A* 115 (2011) 11689.
- [37] T. Liu, B.H. Xia, X. Zhou, H.X. Zhang, Q.J. Pan, J.S. Gao, *Organometallics* 26 (2007) 143.
- [38] B. Minaev, V. Minaeva, H. Agren, *J. Phys. Chem. A* 113 (2009) 726.
- [39] A. Kadari, A. Moncomble, I. Ciofini, M. Brahimi, C. Adamo, *J. Phys. Chem. A* 115 (2011) 11861.
- [40] S.K. Leung, K.Y. Kwok, K.Y. Zhang, K.K.W. Lo, *Inorg. Chem.* 49 (2010) 4984.
- [41] T. Hofbeck, H. Yersin, *Inorg. Chem.* 49 (2010) 9290.
- [42] E.E. Langdon-Jones, A.J. Hallett, J.D. Routledge, D.A. Crole, B.D. Ward, J.A. Platts, S.J.A. Pope, *Inorg. Chem.* 52 (2013) 448.
- [43] M. Tavasli, T.N. Moore, Y.H. Zheng, M.R. Bryce, M.A. Fox, G.C. Griffiths, V. Jankus, H.A. Al-Attar, A.P. Monkman, *J. Mater. Chem.* 22 (2012) 6419.
- [44] S. Okada, K. Okinaka, H. Iwakaki, M. Furugori, M. Hashimoto, T. Mukaide, J. Kamatani, S. Igawa, A. Tsuboyama, T. Takiguchi, K. Ueno, *Dalton Trans.* 9 (2005) 1583.
- [45] A.B. Tamayo, B.D. Alleyne, P.I. Djurovich, S. Lamansky, I. Tsyba, N.N. Ho, R. Bau, M.E. Thompson, *J. Am. Chem. Soc.* 125 (2003) 7377.
- [46] J. Brooks, Y. Babayan, S. Lamansky, P.I. Djurovich, I. Tsyba, R. Bau, M.E. Thompson, *Inorg. Chem.* 41 (2002) 3055.
- [47] S.D. Cummings, R.J. Eisenberg, *J. Am. Chem. Soc.* 118 (1996) 1949.
- [48] A.J. Lees, *Comments Inorg. Chem.* 17 (1995) 319.
- [49] S.C. Chan, M.C.W. Chan, Y. Wang, C.M. Che, K.K. Cheung, N.Y. Zhu, *Chem. Eur. J.* 7 (2001) 4180.
- [50] M.A. Baldo, C. Adachi, S.R. Forrest, *Phys. Rev. B* 62 (2000) 10967.
- [51] E.B. Namdas, A. Ruseckas, D.W. Samuel, S.C. Lo, P.L. Burn, *Appl. Phys. Lett.* 86 (2005) 091104.